In-plane and out-of-plane transverse susceptibility in close-packed arrays of monodisperse Fe nanoparticles

P. Poddar, J. L. Wilson, and H. Srikanth*
Materials Physics Laboratory, Department of Physics, University of South Florida, Tampa, Florida 33620, USA

D. F. Farrell and S. A. Majetich
Department of Physics, Carnegie Mellon University, Pittsburgh, Pennsylvania 15213, USA
(Received 16 June 2003; published 8 December 2003)

The transverse susceptibility (TS) of arrays of self-assembled Fe nanoparticles has been studied using a sensitive radio-frequency resonant technique. Symmetrically located broad peaks in the TS data are observed below the blocking temperature as the applied field is swept from positive to negative saturation. These peaks occur at the effective anisotropy fields ($\pm H_K$) with the peak width determined by the distribution in H_K in the nanoparticle array system. These features are observed to be strongly affected by dipolar interactions as well as thermal relaxation. Systematically tracking the evolution of the TS curves across the superparamagnetic transition reveals distinct temperature ranges over which thermal activation and dipolar energy overcome the effective magnetic anisotropy energy. Hysteresis loops measured using a superconducting quantum interference device magnetometer indicate a smaller coercive field for in-plane field orientation compared to that for out-of-plane orientation. This is also reflected in the TS measurements. A comparison of the TS over a wide range in temperature and magnetic fields, applied in plane and out of plane, reveals the distinct influence of variation in dipolar interaction strengths for the two geometries.

DOI: 10.1103/PhysRevB.68.214409 PACS number(s): 75.20.−g, 75.30.Gw, 75.50.Tt, 75.75.+a

INTRODUCTION

Ordered arrays of magnetic nanoparticles have promising technological applications. The study of static and dynamic magnetic properties of these systems is extremely interesting because of their potential use in magnetic random access memory, high-density magnetic memory storage devices, magnetic read-head sensors, magnetic switches, etc.[1–3] Surfactant-coated particles are known to be ideal for developing self-assembled passivated nanocrystal superlattices or nanocrystal arrays of metal, semiconductor, and oxide clusters.[4] Recently, several methods have been developed to produce highly crystalline, monodisperse, magnetic nanoparticles using wet chemical approach like sol-gel, reverse micelle, coprecipitation, sonochemistry, etc.[5–7]

For nearly five decades, there have been various pioneering studies on superparamagnetic particles in the form of ferrofluids, which has contributed significantly towards the understanding of the interparticle interactions and spin relaxation.[8–11] A recent such study of a three-dimensional (3D) system of highly uniform, chemically synthesized cobalt nanoparticles shows that it is possible to calculate the distribution of anisotropy energy as well as magnetically active volume by simultaneous modeling of remanent and field-induced magnetization data.[12] It was also established in this study that the variations in the shapes of the magnetic cores of the nanoparticles generate the anisotropy which governs the blocking process.

Due to the potential application in high-density memory storage, there is current interest in studying the role of interparticle dipolar interactions, switching fields, spin relaxation, and anisotropy field behavior in close-packed monolayer and multilayer arrays of monodisperse particles. Techniques like the dip-coating, drop-casting, spin-coating, and Langmuir-Blodgett techniques are various ways to self-assemble nanoparticles. It is known that the blocking temperature of the magnetic nanoparticle systems also strongly depends upon the interparticle interactions and particle size distribution. These self-assembly techniques allow random orientation of surfactant-coated particles. Moreover, due to the coating, these particles have negligible exchange interaction between them and the magnetic behavior is largely determined by dipolar interactions.

In this study, we have chosen a very sensitive and precise rf technique to probe the transverse susceptibility (TS) in close-packed multilayer arrays of surfactant-coated iron nanoparticles. In TS experiments, typically a small perturbing ac or rf field is applied to the sample in addition to the swept dc magnetic field. Over the years, this technique has been popular among researchers working on multidomain and single-domain particle systems such as magnetic tapes, inks, etc., due to its capability of directly probing the anisotropy field.[13] The multidomain and single-domain particles exhibit different field-dependent TS characteristics due to the presence or absence of the domain wall displacement mechanism.[14] However, most of these studies were adversely affected by unwanted texturing of samples and the presence of multidomain particles. The role of texture on the TS has also been investigated in detail.[15] A maximum entropy approach has been used to show that it is possible to calculate the anisotropy field distribution function from the experimental peak width.[16]

To our knowledge, there is no systematic TS study on close-packed monolayer or multilayers of superparamagnetic particles. The control achieved recently in synthesizing highly monodisperse, single-crystalline nanoparticles not

only makes it possible to test existing theoretical predictions but also provides opportunities for conducting experiments resulting in high quality data for future theoretical work. It has generally been difficult to resolve the effects of interparticle interactions, particle size dispersion, and thermal effects at different temperatures above and below the blocking temperature. The introduction of our rf method based on a slightly different approach to measure TS resulted in increased precision, thus providing an opportunity to address these issues. The rf experiments and theoretical analysis of TS in γ-Fe_2O_3 nanoparticles have been presented elsewhere.[17]

The first detailed theory of TS was due to Aharoni *et al.* and was based on the Stoner-Wohlfarth formalism.[18,19] However, this theory is strictly applicable for the ideal case of noninteracting single-domain magnetic particles and does not take into consideration interparticle interactions, particle size and shape dispersion, and relaxation effects. Aharoni *et al.* suggested that for a unipolar field scan from positive to negative saturation, the transverse susceptibility reveals three singularities, two of them at the anisotropy fields ($\pm H_K$) and one at the switching field. However, most of the experimental studies usually report two symmetric peaks located at the anisotropy fields and the third peak is often broadened and merged with one of these peaks due to a large distribution in particle size. Finite-temperature effects and the influence on the peak shapes have also been addressed in the context of the model of Aharoni *et al.*[17]

The aim of this study is to explore the physics of magnetic interactions in a close-packed multilayer (nearly 15 layers) structure of single-domain Fe particles through radio-frequency TS experiments. A comparison of the TS with the *M-H* characteristics measured in a superconducting quantum interference device (SQUID) magnetometer is also presented. To our knowledge, this is the first study of TS on monodisperse magnetic nanoparticle arrays.

SYNTHESIS AND CHARACTERIZATION

Monodisperse surfactant-coated Fe nanoparticles were prepared by high-temperature decomposition of iron pentacarbonyl. The synthesis details are presented elsewhere.[20] The particles are coated with a thin layer (approximately 1 nm) of oleic acid to avoid agglomeration. This results in a surface layer of iron oxide, a few Å thick, leading to a reduction in surface moments. The particles contain approximately 2 wt % carbon impurities, and electron diffraction shows a bcc pattern with broadened rings indicating some structural disorder, leading to a lower magnetic moment than a comparable volume of bulk iron.[21] In Fig. 1, we have shown the transmission electron micrograph (TEM) of as-synthesized iron nanoparticles. For this purpose, a drop of volatile solvent containing Fe nanoparticles is allowed to slowly evaporate on a carbon-coated TEM grid at room temperature. Usually the low boiling point of the solvents allows for slow evaporation. This added thermal energy permits the particles to diffuse to their lowest-energy sites during the evaporation, producing a well-organized monolayer of particles.[22] The TEM micrograph of the 2D array shows that particles are

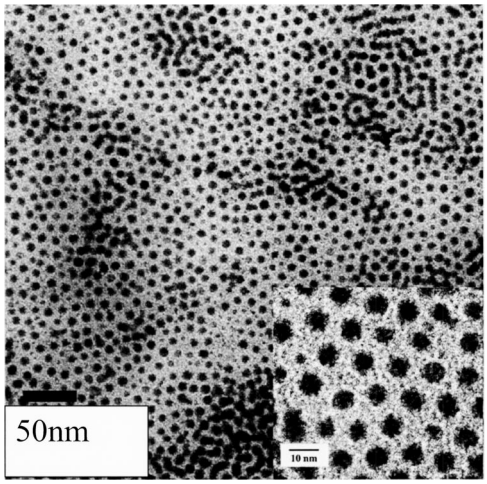

FIG. 1. Transmission electron micrograph of the iron particles. Inset shows a closer view of short-range ordering.

almost monodisperse with an average size of 6.8 ± 1.6 nm.

For the magnetization measurements, carbon-coated nylon TEM grids were dipped into a solution containing iron nanoparticles, which resulted in deposition of nearly 15 close-packed monolayer thick coatings over the grids. TEM studies of similar samples revealed short-range (nearest neighbor to 50 nm length scale) ordering of particles, but in the long range the morphology was more disordered. The sample handling was done in an inert environment. For magnetic measurements, a stack of ten such TEM grids was bonded to increase the overall signal and the whole stack was encased in silicon grease to protect it from oxidation. This stack of TEM grids was placed in a gelatin capsule and was used in magnetic measurements with a SQUID as well as the rf transverse susceptibility experiments.

STATIC AND DYNAMIC MAGNETIC MEASUREMENTS

Static magnetic characterization was done using a Quantum Design SQUID magnetometer. In Fig. 2, we present the field-cooled (FC) and zero-field-cooled (ZFC) magnetization at 200 Oe for field orientations parallel and perpendicular to the sample surface. The curves display a peak at around 75 K for a dc magnetic field applied parallel to the plane of the TEM grids and at 65 K for a magnetic field perpendicular to

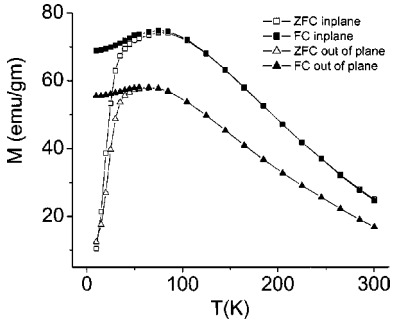

FIG. 2. Field-cooled and zero-field-cooled magnetization measured at 200 Oe using a SQUID magnetometer. For comparison, the data for in-plane ($\parallel$) and out-of-plane ($\perp$) orientations are plotted.

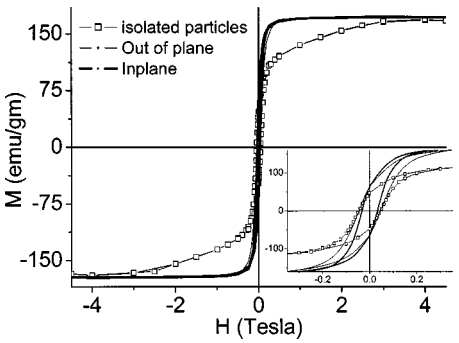

FIG. 3. M-H curves for in-plane ($\parallel$) and out-of-plane ($\perp$) field orientations measured with a SQUID at 10 K for a stack of TEM grids with dip-coated nanoparticle arrays. Data for a dilute suspension of particles are also shown for comparison. Inset shows a zoom view of the hysteresis loops.

the plane. This is the characteristic signature of the transition from a superparamagnetic state at high temperatures to a state where the spins are blocked. In Fig. 3, we show the M-H measurements done at 10 K using a SQUID magnetometer for both field orientations. For comparison, the data for a highly dilute suspension of nearly isolated Fe nanoparticles are also shown. The results show that the in-plane coercivity ($H_C^{\parallel}$) is 325 Oe whereas the out-of-plane coercivity ($H_C^{\perp}$) is 450 Oe. The M-H results also indicate that the ratio of remanent to saturation magnetization (M_R/M_S) is around 0.38 and remains the same for both orientations. The M_R/M_S ratio is 0.29 for the dilute sample. The saturation magnetization calculated from these curves is between 168 and 171 emu/g. In the inset, it can be observed that the curve corresponding to the in-plane field orientation rises much more steeply than other curves.

To study the effect of the in-plane and out-of-plane field orientations directly on the effective magnetic anisotropy, we conducted TS experiments using a resonant rf technique based on a tunnel-diode oscillator (TDO).[23] This method has been validated by us over the years to be an excellent probe of the dynamic magnetic response and, in particular, the anisotropy. In this technique, a small fixed-amplitude (<5 Oe) rf (10 MHz) field is applied parallel or perpendicular to the variable external dc field and the parallel (χ_P) and transverse (χ_T) components of susceptibility can be independently resolved. Since the sample is placed in an inductive rf coil that is part of a self-resonant circuit, the shift in the resonant frequency with varying dc field and/or temperature gives a direct measure of the change in inductance and thus the sample susceptibility. The error in measurement of the resonant frequency shift using an HP frequency counter is only 1–10 Hz. Therefore, this experiment provides a very precise way to study the field dependence of susceptibility. The background due to the empty coil is negligible and can be subtracted to extract the change in susceptibility due to the magnetic specimen. A schematic of the transverse susceptibility setup is shown in the top section of Fig. 4. The capacitive portion of the LC resonant circuit is located at room temperature and the inductive coil with the sample is attached to the end of a homemade semirigid coaxial cable

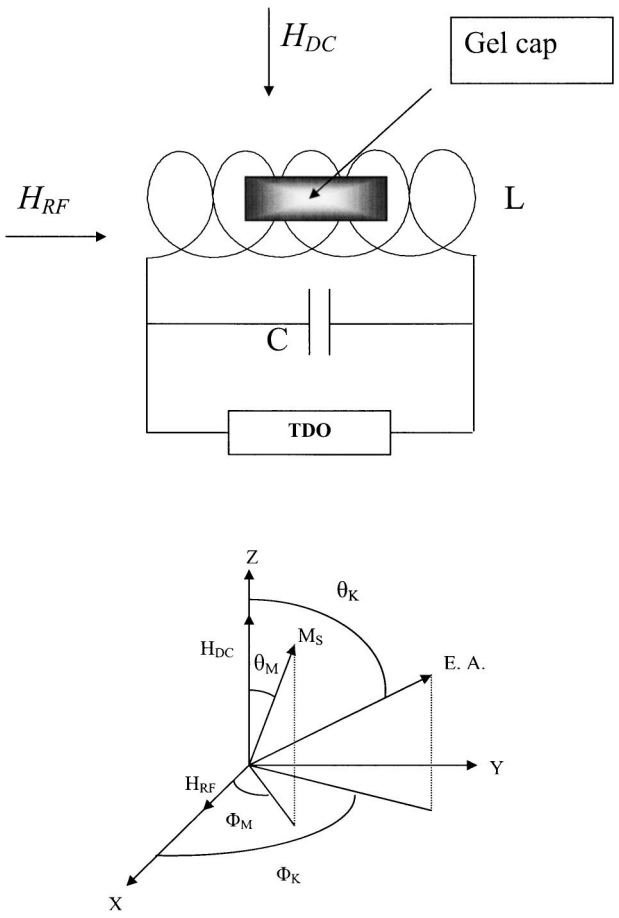

FIG. 4. (Top) Schematic of the TDO-based TS measurement geometry. (Bottom) Schematic representation showing magnetization, easy axis, rf, and dc field directions for the TS configuration.

insert that is designed to fit into the sample space of a commercial physical property measurement system (PPMS) from Quantum Design. The nylon TEM grids as well as the gelatin capsule have a diamagnetic background but its contribution to transverse susceptibility measurements is not significant. The TS measurements were done for two different dc field orientations with respect to the sample surface: $\chi_T^{\parallel}$ represents the TS in the plane of the sample and $\chi_T^{\perp}$ out of plane of the sample. Measurement geometries for different susceptibility components χ_P, $\chi_T^{\perp}$, and $\chi_T^{\parallel}$ are schematically shown in Fig. 5. The rf transverse susceptibility data are plotted as a percentage change since this is directly extracted from the change in resonant frequency measured with an HP frequency counter.[17] By using the precise geometrical parameters and estimating the fill factor, the absolute values of χ_P and χ_T can be determined. However, for the purpose of the present study in which our intent is to follow the TS variation as a function of field and temperature, we have plotted the parallel and transverse susceptibilities using the following relation:

$$\left(\frac{\Delta\chi}{\chi}\right)\% = \frac{[\chi(H)-\chi^{sat}]\times 100}{\chi^{sat}},$$

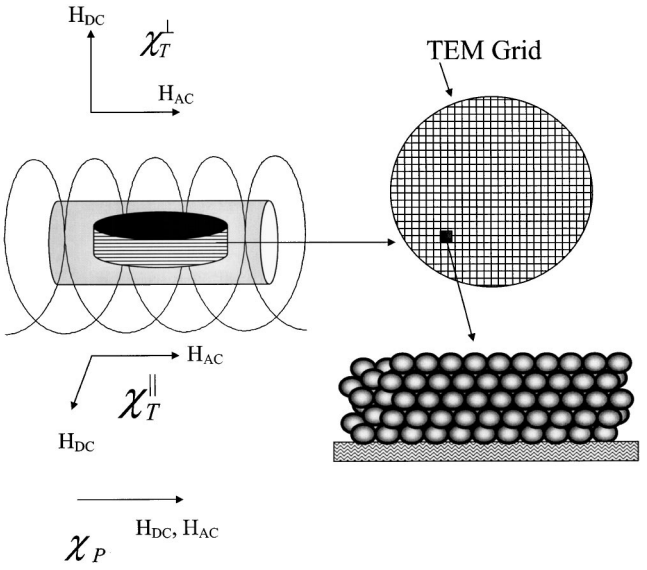

FIG. 5. Schematic representation of the sample in coil and the different orientations of the dc and rf fields with respect to the sample surface to realize the parallel case (χ_P) and the two transverse cases ($\chi_T^{\perp}$ and $\chi_T^{\parallel}$). All the field directions are with respect to the longitudinal axis of the coil.

where, χ^{sat} is the extrapolated value of the TS at high fields where the slope is close to zero.

It is relevant here to distinguish between the parallel and transverse susceptibilities. It is known that only transverse susceptibility is able to directly resolve the anisotropy peaks. This has been discussed back in 1957 in a classic paper by Aharoni *et al.*[18] In the bottom part of Fig. 4, we have shown a schematic 3D polar plot representation showing the effective magnetization vector subject to Zeeman and magnetocrystalline terms under the conditions of TS experimental geometry. For the dc magnetic field applied along the z direction, the parallel susceptibility is given by

$$\chi_P = \frac{dM_Z}{dH_Z},$$

where $H_X = H_Y = 0$ and the transverse susceptibility term is given as

$$\chi_T = \left(\frac{dM_x}{dH_z}\right)_{H_X=0}, \quad H_Y = 0.$$

Based on the coordinate system given in Fig. 4, the mean value of the parallel and transverse susceptibilities for a single-domain particle with uniaxial anisotropy can be written as

$$\overline{\chi_P} = \frac{3}{2}\int_0^{\pi/2}\left[\frac{\sin^2\theta_M \sin\theta_K}{h\cos\theta_M + \cos 2(\theta_M - \theta_K)}\right] d\theta_K,$$

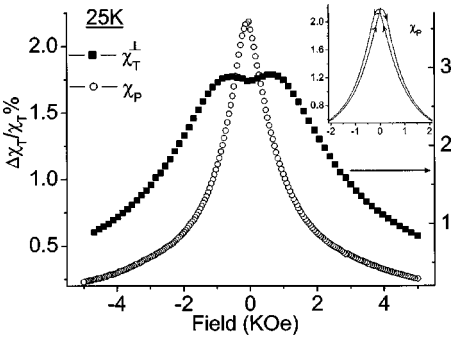

FIG. 6. The difference in the parallel (χ_P) and transverse susceptibility ($\chi_T^{\perp}$) at 25 K is shown. The TS data show distinct peaks associated with the effective anisotropy fields.

$$\overline{\chi_T} = \frac{3}{4}\chi_0\int_0^{\pi/2}\left[\frac{\cos^2\theta_M}{h\cos\theta_M + \cos 2(\theta_K - \theta_M)} + \frac{\sin(\theta_K - \theta_I)}{h\sin\theta_K}\right]\sin\theta_K d\theta_K,$$

where h is the reduced field (H/H_K). These terms can be numerically calculated for a system of such single-domain particles where randomness in the anisotropy axis orientations and particle size distribution can be incorporated into the expression. In particular, χ_T calculations yield singularities at the anisotropy field (H_K) and this is the basis behind TS experiments where these singularities can be detected. It should be pointed out that TS theories for single-domain nanoparticles consider uniaxial anisotropy alone. Strictly speaking, TS experiments probe the effective anisotropy fields where higher-order magnetocrystalline anisotropy constants, dipolar interactions, surface spin disorder, etc., could contribute to the observed peak structure. In the present case, the Fe nanoparticles have body-centered-cubic (bcc) structure. However, typically in nanoparticles, small variations in particle shape and size are enough to induce a predominantly uniaxial behavior.

To emphasize the distinction between χ_T and χ_P, in Fig. 6 we have plotted both data taken on the Fe nanoarray sample at 25 K. For clarity, we have shown the data in the main panel for unipolar field sweeps (from positive to negative field). For the ease of identification of the peaks, we will also refer to the positive and negative sections in the graphs as the first and second quadrants, respectively. It can be seen that the TS curve shows two prominent symmetric peaks in the first and second quadrants ($\sim \pm 600$ Oe). The parallel susceptibility data for the same sample shown for comparison do not show peaks at the effective anisotropy fields but instead show peaks at much lower field values corresponding to the switching fields. The nature of the χ_P peaks is different; i.e., starting from positive saturation (first quadrant), the peak is located in the second quadrant and vice versa. This ''crossover'' peak behavior is illustrated in the inset of Fig. 6, which shows the low-field χ_P data for a bipolar field scan covering the full loop (positive saturation→negative saturation→positive saturation). Note that the peaks in χ_P occur at switching fields identified as regions where the

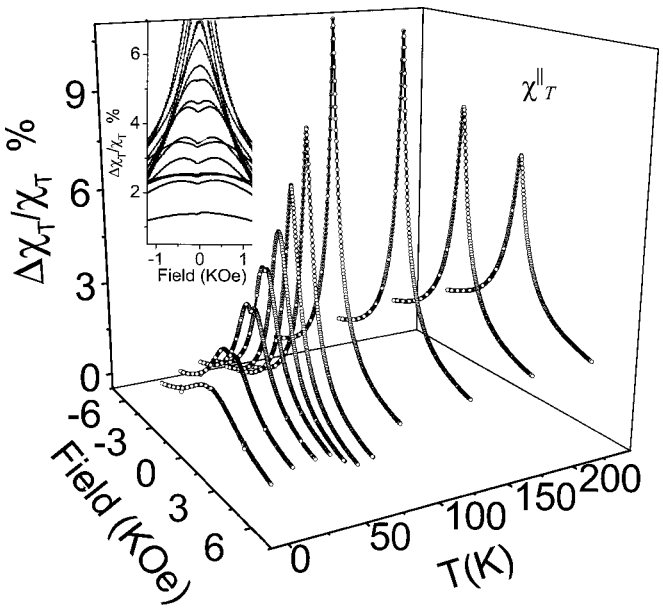

FIG. 7. In-plane transverse susceptibilities ($\chi_T^{\parallel}$) for a wide range of temperature. Data in main panel are for a unipolar field scan from $+5$ to -5 kOe. Inset shows the same curve plotted differently to highlight the peak behavior.

maximum change in slope occurs in the M-H hysteresis loops. Thus, these field values are smaller than the coercive fields (which are strictly intercepts on the x axis) and overall consistent with the SQUID data.

The focus in the rest of the paper is on the TS data with the dc field applied in plane and out of plane to the sample surface. As mentioned earlier, the field dependence of TS of ingle-domain particles based on Stoner-Wohlfarth model exhibits singularities at the effective anisotropy fields. These peaks are noticeable in the TS data shown in Fig. 6 but they are considerably broadened because of the distribution in particle size and anisotropy fields of the collection of particles making up the arrays.

In Fig. 7, we have mapped the TS curves for in-plane orientation ($\chi_T^{\parallel}$) (see the schematic in Fig. 5 for the field orientations). This family of curves traces the evolution of the system across the ferromagnetic-superparamagnetic transition as the temperature is increased. In fact, the envelope of the zero-field ($H_{dc}=0$) TS has a maximum around 100 K, which we ascribe to the blocking temperature under TS experimental conditions. Below and above this temperature the zero-field TS decreases sharply. It is well known that the signature of the blocking temperature depends on the experimental conditions like time scale, application of an external field, etc. So one should be cautious in comparing the blocking temperature measured using TS and SQUID susceptibility experiments. As the temperature is lowered and at around 55 K, the single peak in the TS at zero field splits into two peaks, which become more prominent with decreasing temperature and shift to higher field values. These peaks represent singularities due to the anisotropy fields as discussed before. In the inset, we have shown the development of anisotropy peaks by showing the 2D plot of the same curve

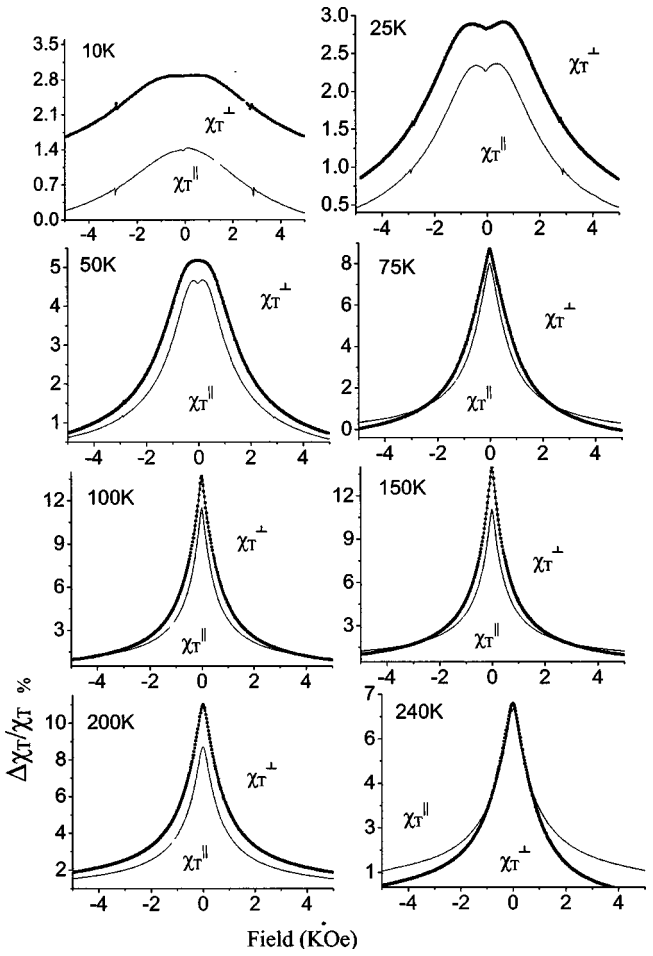

FIG. 8. Frame-by-frame comparative view of $\chi_T^{\perp}$ and $\chi_T^{\parallel}$ curves at temperatures above and below the blocking temperature.

over a smaller field range. The influence of dipolar interactions and thermal relaxation on these peaks is discussed in detail later in the paper.

In Fig. 8, we have compared the transverse susceptibility for two different dc field orientations (in-plane $\chi_T^{\parallel}$ and out-of-plane $\chi_T^{\perp}$) at different temperatures. It can be seen that both curves are almost identical at 240 K except at higher field values. Quantitative comparison of the curves for the two geometries is difficult, as the field orientation cannot be changed *in situ*. The insert is warmed to room temperature to manually change the coil orientation with respect to the dc field. However, qualitatively distinct difference in shape of the TS curves for the two orientations is consistently observed at various temperatures. While cooling down, it can be seen that the peak is generally much broader for $\chi_T^{\perp}$ than for $\chi_T^{\parallel}$ throughout the temperature range. This is consistent with the M-H curves shown in Fig. 3. The approach to saturation is much slower for the out-of-plane orientation.

Below 75 K, the peaks split into two for both cases but the difference between $\chi_T^{\perp}$ and $\chi_T^{\parallel}$ tends to increase. At 10 K, the difference between the two curves is very prominent. The $\chi_T^{\perp}$ curve has much broader peaks in comparison to the $\chi_T^{\parallel}$. The overall broadening of the TS curves may be due to the fact that below the blocking temperature, spins are frozen

randomly resulting in a spin-glass-like state. In a small reverse field, most of the magnetic material switches, but there could be strongly coupled particles forming clusters that switch over a broad range of H. The larger the cluster, the harder it is to switch analogous to the situation in a spin glass or amorphous ferromagnet. Recent evidence from neutron scattering experiments confirms a spin-glass-like behavior in these systems in the blocked state.[24]

The above results can be explained based on the difference in contributions of the dipolar interactions between particles to the TS data for the two different field orientations. The total effective energy of such an interacting particle system can be given by the following expression:

$$E = \frac{\mu^2}{d^3}\sum_{i,j}\frac{(\hat{\mu}_i\cdot\hat{\mu}_j)-3(\hat{\mu}_i\cdot\hat{R}_{ij})(\hat{\mu}_j\cdot\hat{R}_{ij})}{R_{ij}^3}$$

$$-KV\sum_i(\hat{\mu}_i\cdot\hat{e}_i)^2-\mu H\sum_i(\hat{\mu}_i\cdot\hat{H}).$$

The first term here represents the interparticle dipolar interaction energy where μ is the magnetic moment of each particle, R_{ij} is thecenter to center distance between the ith and jth particles measured in units of nearest-neighbor distance d, and $\hat{\mu}_i$ and $\hat{\mu}_j$ are the spin directions of the ith and jth spins. The second term represents the anisotropy energy where K is the anisotropy constant and V is the volume of each particle; $\hat{e}_i$ is the easy axis direction. The third term represents the Zeeman energy where $\hat{H}$ is the magnetic field direction. In this expression, dispersion in particle size has not been taken into account. In the present case of a close-packed multilayer, the overall magnetization behavior is governed by individual particles as well as the collective response of the strongly coupled larger cluster of particles. Because of the close packing, the interparticle dipolar interaction energy which favors in-plane alignment of spins dominates over the individual particle activation energy which favors a 3D disordered state.[25] However, due to the quasi-2D geometry of the sample, there are more particles with strong nearest-neighbor interactions in the plane of the TEM grid than out of plane. The TEM studies show a long-range (more than 50 nm) in-plane order. This introduces a strong in-plane demagnetization field as the effective activation energy is minimized when spins are oriented in the plane of the grid in comparison to the out-of-plane orientation.[25,26]

In several previous studies of 2D and 3D systems, where the effects of introducing the interaction between the superparamagnetic particles were studied, the zero-field-cooled curves showed a much sharper superparamagnetic-ferromagnetic transition peak for the interacting system than for the isolated one.[27] As for the noninteracting particle system, the blocking temperature of every spin is determined solely by its respective activation energy KV. On the other hand, for interacting systems the collective freezing of spins overcomes the individual particle blocking processes.[10] We believe that for the case of strongly interacting particles (such as the system presented here), one is likely to see a noticeable change in the blocking temperature as well. It should be pointed out that the case of weakly or strongly interacting nanoparticle arrays is different from the case of continuous thin films of ferromagnetic materials. In the case of films, the difference between in-plane and out-of-plane magnetization behavior is due to competition between the surface magnetocrystalline anisotropy (generally out of plane) and dipolar interactions, which favor in-plane alignment of spins. Our TS data afford a very sensitive way to systematically monitor changes in the in-plane and out-of-plane cases with decreasing temperature, as presented in Fig. 8.

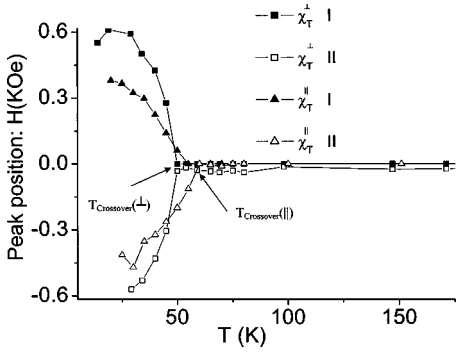

FIG. 9. The field positions of the anisotropy peaks in both quadrants (presented as I for the first quadrant and II for the second quadrant) as a function of temperature. The two peaks resolved at low temperatures merge into a single peak at a temperature ($T_{\text{crossover}}$) that is different for $\chi_T^{\parallel}$ and $\chi_T^{\perp}$ geometries.

The general field and temperature variation of TS shown in Fig. 7 has been observed by us in similar measurements on many other nanoparticle systems and is characteristic of systems undergoing temperature-driven superparamagnetic transitions.[14,28,29] In contrast, similar transverse susceptibility measurements done using the same setup on continuous ferromagnetic thin films of CrO_2 did not show any broadening of TS curves in the temperature range from 300 to 10 K due to the absence of superparamagnetic behavior.[30]

A striking feature of the TS data is the strong temperature dependence of the two-peak structure at low temperatures that we associate with the effective anisotropy field. In a bid to track characteristic features in the TS as a function of temperature, we have plotted the peak position in both the quadrants for in-plane and out-of-plane field orientations in Fig. 9. The out-of-plane peak positions are given by solid and open squares for first and second quadrants, respectively. Peak positions for in-plane measurements are given by solid and open triangles for first and second quadrants, respectively. It can be seen that for $\chi_T^{\perp}$ orientation, the anisotropy peaks are situated at much higher values in comparison to $\chi_T^{\parallel}$. At low temperatures, where thermal effects are insignificant, the anisotropy field is given by the relation $H_K = 2K/M_S$ where K is the first-order anisotropy constant and M_S is the saturation magnetization. The value of M_S is approximately 170 emu/g and the anisotropy constant K is 3.4×10^5 erg/cc. (Ref. 20) From the above the relation, the value of H_K is around 500 Oe. This is in good agreement with the anisotropy fields directly measured with our TS experiments at 25 K or lower. However, in this calculation, higher-order anisotropy constants are not considered and

they are known to be significant in some cases. A recent theoretical study shows the influence of second-order anisotropy energy on uniaxial ferromagnets.[31] It should be noted that peaks are also strongly affected by the dipolar interactions. Ideally, to extract the magnetocrystalline anisotropy of the material, the measurements should be done on an isolated particle system, well below the blocking temperature. Our present study is to demonstrate the precision in TS measurements and the ability to trace the collective response of a superparamagnetic system in the presence of dipolar and Zeeman energies. Systematic experimental investigations have been reported on well-dispersed CrO_2 powder samples to probe the effect of varying interaction on the transverse susceptibility peaks and it was demonstrated that a reduction in the packing fraction of the particles results in a linear increase of anisotropy field.[32]

In Fig. 9, it can be seen that as the temperature is increased, the two peaks in TS close in and merge into a single peak even below the blocking temperature. This strong temperature dependence cannot be accounted for by the thermal variation of the magnetocrystalline anisotropy constant alone. In addition, at any given finite temperature one should also consider the influence of thermal energy that overcomes the anisotropy energy for some particles, thus making them superparamagnetic. So the picture that emerges is that at very low temperatures, most of the particles are frozen (albeit randomly and some in clusters). As the temperature is increased, an increasing fraction of the total number of particles becomes superparamagnetic. Above the blocking temperature, all the particles are superparamagnetic, yielding the well-known $1/T$ dependence in susceptibility. To our knowledge, TS experiments appear to be the most sensitive probes of the influence of thermal energy as we have consistently seen this general behavior in a number of superparamagnetic systems. Again, to emphasize the point that this is characteristic of nanoparticles, we have confirmed that the anisotropy peak fields in TS experiments on continuous ferromagnetic thin films of CrO_2 do not show any strong temperature dependence.[30] In Fig. 9, the anisotropy peaks in the first and second quadrants merge at 55 K and 65 K for $\chi_T^{\perp}$ and $\chi_T^{\parallel}$, respectively. Since the blocking temperatures for TS experiments are shifted to higher values (i.e., 100 K for in-plane orientation), we identify these new temperature scales ($T_{\text{crossover}}$) of 65 K and 55 K at which the TS double-peak structure merges into a single peak at zero field as yet another crossover region within the blocked state but in proximity to the ferromagnetic-superparamagnetic transition. It should be remembered that blocking temperatures measured from SQUID ZFC-FC curves were 65 K and 75 K for out-of-plane and in-plane field orientations, respectively. Quantitative analyses of the significance of these crossover temperatures require further experiments on other systems. However, qualitatively one can understand it as follows. $T_{\text{crossover}}$, which is different for in-plane and out-of-plane orientations, is the temperature above which the effective anisotropy energy of the system is overcome by thermal energy. However, weak short-range particle nteractions persist up to the blocking temperature (T_B). It is only above T_B that true superparamagnetic behavior characterized by random thermal fluctuations of single-domain particle moments is realized. We believe that the presence of $T_{\text{crossover}}$ is clearly observed in TS experiments because of the sensitivity of this technique in directly measuring the influence of effective magnetic anisotropy.

SUMMARY

We have conducted in-plane and out-of-plane transverse susceptibility measurements on close-packed arrays of Fe nanoparticles. The evolution of the transverse susceptibility peaks below the blocking temperature can be mapped and shows a distinct difference with respect to the field orientations. Overall, our results are consistent with SQUID magnetization measurements and indicate the role of interactions and possibly other collective phenomena in the blocked state.

ACKNOWLEDGMENTS

H.S. acknowledges support from the NSF through Grant No. ECS-0140047. S.A.M. acknowledges support from the NSF through Grant. No. CTS-0227645 and from the American Chemical Society Petroleum Research Fund through Grant. No. ACS-PRF-37578-AC5.

*Corresponding author. Electronic address: sharihar@cas.usf.edu

[1] C. T. Black, C. B. Murray, R. L. Sandstrom, and S. Sun, Science **290**, 1131 (2000).
[2] R. P. Cowburn, Science **287**, 1466 (2000).
[3] R. L. White, R. M. H. New, and R. F. W. Pease, IEEE Trans. Magn. **33**, 990 (1997).
[4] Z. L. Wang, Adv. Mater. (Weinheim, Ger.) **10**, 13 (1998).
[5] T. Sugimoto and E. Matijevic, J. Colloid Interface Sci. **74**, 227 (1980).
[6] K. M. Lee, C. M. Sorensen, K. J. Klabunde, and G. C. Hadjipanayis, IEEE Trans. Magn. **28**, 3180 (1992).
[7] X. Cao, Yu. Koltypin, G. Kataby, R. Prozorov, and A. Gedanken, J. Mater. Res. **10**, 2952 (1995).
[8] W. Luo, S. Nagel, T. F. Rosenbaum, and R. E. Rosenzweig, Phys. Rev. Lett. **67**, 2721 (1991).
[9] T. Jonsson, P. Svedlindh, and M. F. Hansen, Phys. Rev. Lett. **81**, 3976 (1998).
[10] J. L. Dormann, D. Fiorani, and E. Tronc, Adv. Chem. Phys. **98**, 283 (1997).
[11] J. Zhang, C. Boyd, and W. Luo, Phys. Rev. Lett. **77**, 390 (1996).
[12] G. A. Held, G. Grinstein, H. Doyle, S. Sun, and C. B. Murray, Phys. Rev. B **64**, 012408 (2001).
[13] A. A. Potanin, S. M. Shrauti, D. W. Arnold, and A. M. Lane, J. Appl. Phys. **81**, 3803 (1997).
[14] L. Pareti and G. Turilli, J. Appl. Phys. **61**, 5098 (1987).
[15] P. M. Sollis, P. R. Bissell, and R. W. Chantrell, J. Magn. Magn. Mater. **155**, 123 (1996).
[16] R. W. Chantrell, P. R. Bissell, P. Sollis, A. Hoare, and T. Orth, J. Magn. Magn. Mater. **177–181**, 894 (1998).
[17] L. Spinu, C. J. O'Connor, and H. Srikanth, IEEE Trans. Magn. **37**, 2188 (2001).
[18] A. Aharoni, E. H. Frei, S. Shtrikman, and D. Treves, Bull. Res.

Counc. Isr., Sect. F **6A**, 215 (1957).
[19] E. C. Stoner and E. P. Wohlfarth, Proc. R. Soc. London, Ser. A **240**, 599 (1948).
[20] K. D. Humfeld, A. K. Giri, S. A. Majetich, and E. L. Venturini, IEEE Trans. Magn. **37**, 2194 (2001).
[21] R. V. Chamberlin, K. D. Humfeld, D. Farrell, S. Yamamuro, Y. Ijiri, and S. A. Majetich, J. Appl. Phys. **91**, 6961 (2002).
[22] V. F. Puntes, K. M. Krishnan, and P. Alivisatos, Appl. Phys. Lett. **78**, 2187 (2001).
[23] H. Srikanth, J. Wiggins, and H. Rees, Rev. Sci. Instrum. **07**, 3097 (1999).
[24] S. A. Majetich (private communication).
[25] V. Russier, J. Appl. Phys. **89**, 1287 (2001).
[26] V. Russier, C. Petit, J. Legrand, and M. P. Pileni, Appl. Surf. Sci. **164**, 193 (2000).
[27] P. Poddar, T. T.-Shafir, T. Fried, and G. Markovich, Phys. Rev. B **66**, 060403 (2002) and references therein.
[28] H. Srikanth, E. E. Carpenter, L. Spinu, J. Wiggins, W. L. Zhou, and C. J. O'Connor, Mater. Sci. Eng., A **304–306**, 901 (2001).
[29] H. Srikanth, Mater. Phys. Mech. **4**, 1 (2001).
[30] L. Spinu, H. Srikanth, A. Gupta, X. W. Li, and G. Xio, Phys. Rev. B **62**, 8931 (2000).
[31] L. Spinu, A. Stancu, C. J. O'Connor, and H. Srikanth, Appl. Phys. Lett. **80**, 276 (2002).
[32] P. M. Sollis, P. R. Bissell, and Y. Matsutake, IEEE Trans. Magn. **33**, 3046 (1997).